Published in final edited form as:
Int J Radiat Oncol Biol Phys. 2011 June 1; 80(2): 574–581. doi:10.1016/j.ijrobp.2010.12.028.

In vivo near-infrared spectroscopy and MRI monitoring of tumor response to Combretastatin A-4-phosphate correlated with therapeutic outcome

Dawen Zhao, M.D., Ph.D.[1], **Cheng-Hui Chang, Ph.D.**[2], **Jae G. Kim, Ph.D.**[3], **Hanli Liu, Ph.D.**[3], and **Ralph P. Mason, Ph.D.**[1,3]

[1]Department of Radiology, UT Southwestern Medical Center, Dallas, TX

[2]Department of Radiation Oncology, UT Southwestern Medical Center, Dallas, TX

[3]Joint Program of Biomedical Engineering, UT Arlington and UT Southwestern Medical Center, Arlington, TX

Abstract

Purpose—To develop a combination treatment of Combretastatin A-4-phosphate (CA4P) with radiation based on tumor oxygenation status.

Methods and Materials—*In vivo* near-infrared spectroscopy (NIRS) and diffusion-weighted (DW) MRI were applied to non-invasively monitor tumor blood oxygenation change and necrosis induced by CA4P (30 mg/kg) in rat mammary 13762NF adenocarcinomas and the evidence used to optimize combinations of CA4P and radiation treatment (a single dose of 5 Gy).

Results—NIRS showed decreasing concentrations of tumor vascular oxyhemoglobin and total hemoglobin during the first 2 h after CA4P treatment, indicating significant reductions in tumor blood oxygenation and perfusion ($p < 0.001$). Twenty-four hours later, in response to oxygen inhalation, significant recovery in tumor vascular and tissue oxygenation was observed by NIRS and pimonidazole staining, respectively ($p < 0.05$). DW MRI revealed significantly increased water diffusion in tumors measured by apparent diffusion coefficient (ADC) at 24 h ($p < 0.05$), suggesting CA4P-induced central necrosis. In concordance with the observation of tumor oxygen dynamics, we found that treatment efficacy depended on the timing of the combined therapy. The most significant delay in tumor growth was seen in the group of tumors treated with radiation, while breathing oxygen 24 h after CA4P administration.

Conclusions—Non-invasive evaluation of tumor oxygen dynamics allowed us to rationally enhance the response to combined treatment of CA4P and radiation on syngeneic rat breast tumors.

Keywords

Combretastatin A-4-phosphate; diffusion-weighted MRI; near-infrared spectroscopy; radiation; hypoxia

Correspondence author: Dawen Zhao, M.D., PhD., Department of Radiology, UT Southwestern, Medical Center, 5323 Harry Hines Blvd. Dallas, TX 75390-9058, Tel: 214-648-9621; Fax: 214-648-4538, Dawen.Zhao@UTSouthwestern.edu.
C-H.C and J.G.K contributed equally to this study.

Conflicts: None.

Introduction

Development of neovascualture is critical for tumor growth, survival, and metastasis, and it has been suggested that vascular disrupting agents (VDA) offer a potential therapy (1,2). Tubulin binding agents, *e.g.*, Combretastatin A-4-phosphate (CA4P), represent a class of VDAs, which selectively cause tumor vascular shutdown and subsequently trigger a cascade of tumor cell death (2,3). Promising preclinical studies have shown that VDAs induce massive necrosis of central tumor tissues. However, a thin rim of tumor cells survives the treatment and it is recognized that a combined therapeutic approach will be required (2). Combined treatment with radiation appears attractive, since radiation should be effective against the surviving rim, which is expected to be relatively better perfused and oxygenated (4). However, efficacy depends on the sequence and interval between radiation and VDA (5). Greater antitumor effects were achieved when VDA was administered 1-3 h after a single dose of radiation, while the enhancement was reduced or lost, if radiation followed shortly after VDA, likely due to increased hypoxia induced by VDA.

Assessment of baseline tumor pathophysiology and dynamic changes in response to treatment ought to provide insight into mechanisms of action and allow rational therapeutic combination (6). We previously showed significantly decreased perfusion by dynamic contrast enhanced (DCE) MRI and increased hypoxia by ^{19}F NMR oximetry in 13762NF breast tumors following CA4P (7). While ^{19}F MRI provides quantitative oximetry with relevant spatial and temporal resolution (8,9), our experience with noninvasive near-infrared spectroscopy (NIRS) and diffusion-weighted (DW) MRI suggested that these methods could also interrogate vascular perfusion, oxygenation and necrosis. Indeed, NIRS can detect relative changes in oxy- and deoxy–hemoglobin concentrations in tissue non-invasively (10,11). Meanwhile, DW MRI, depending on the microscopic mobility of water, has been increasingly used in assessment of tumor pathophysiology and response to various treatment modalities (12,13). We hypothesize that treatment with CA4P and radiation could be enhanced based on *in vivo* observations of temporal tumor oxygenation and the ability to modify tumor hypoxia. We performed 7 different experimental treatment schemes on 13762NF breast tumors with various timing combinations of CA4P and radiation, and with or without oxygen intervention.

Methods

The study was approved by the Institutional Animal Care and Use Committee of UT Southwestern.

Tumor Model

Rat mammary carcinoma 13762NF (Division of Cancer Therapeutics, NCI) was implanted in a skin pedicle surgically created on the foreback of Fisher 344 adult female rats (Harlan), as described in detail previously (7). In brief, the rats were anesthetized and a flap of depilated skin was raised from the back neck/shoulder region. A 3 cm incision was made with a sharp pointed scalpel through both layers of skin using the curved edge of the bulldog clamp as a guide Wound clips (9 mm) were used to join the cut edges of the skin, such that the end result resembled a suitcase handle. After 2 weeks, when the skin had sufficiently healed, the wound clips were removed. At this time, the pedicle was ready for tumor transplantation. A piece of tumor from a donor animal was transplanted into the lumen of the pedicle.

Drug preparation and dosing

Combretastatin A4 phosphate was provided by OXiGENE, Inc. (Waltham, MA) and dissolved in 0.9% saline at a concentration of 30 mg/ml before each experiment.

In vivo monitoring of tumor blood oxygenation

A fiber-based NIRS system consisted of (i) a tungsten-halogen broadband (20W, 360 – 2000 nm) light source (HL-2000-HP, Ocean Optics Inc., Dunedin, FL), (ii) a visible-to-NIR spectrometer (USB2000, Ocean Optics) in the range of 400 – 1000 nm, (iii) a fiber bundle (FiberTech Optica, Kitchener, Ontario, Canada) of 3-mm-core diameter to deliver light from the source to the tumor, and (iv) another 0.6-mm-diameter fiber (Ocean Optics) in a transmittance mode to deliver the collected light from the tumor to the spectrometer. Spectral responses over time were recorded using OoiBase32 software (Ocean Optics). Two wavelengths (750 nm and 830 nm) were used to calculate changes in oxyhemoglobin ($\Delta[HbO_2]$), deoxyhemoglobin ($\Delta[Hb]$) and total hemoglobin ($\Delta[Hb_{total}]$) concentrations. Based on Beer Lambert's law, Eqs. (1-3) were used to estimate changes of $\Delta[HbO_2]$ and $\Delta[Hb]$:

$$\begin{pmatrix} \Delta \mathrm{OD}^{\lambda 1} \\ \Delta \mathrm{OD}^{\lambda 2} \end{pmatrix} = \begin{pmatrix} \varepsilon_{\mathrm{Hb}}^{\lambda 1} & \varepsilon_{\mathrm{HbO_2}}^{\lambda 1} \\ \varepsilon_{\mathrm{Hb}}^{\lambda 2} & \varepsilon_{\mathrm{HbO_2}}^{\lambda 2} \end{pmatrix} \begin{pmatrix} \Delta[\mathrm{Hb}] \\ \Delta[\mathrm{HbO_2}] \end{pmatrix} L \tag{1}$$

$$\begin{pmatrix} \Delta[\mathrm{Hb}] \\ \Delta[\mathrm{HbO_2}] \end{pmatrix} = \frac{1}{d \cdot DPF} \begin{pmatrix} \varepsilon_{\mathrm{Hb}}^{\lambda 1} & \varepsilon_{\mathrm{HbO_2}}^{\lambda 1} \\ \varepsilon_{\mathrm{Hb}}^{\lambda 2} & \varepsilon_{\mathrm{HbO_2}}^{\lambda 2} \end{pmatrix}^{-1} \begin{pmatrix} \Delta \mathrm{OD}^{\lambda 1} \\ \Delta \mathrm{OD}^{\lambda 2} \end{pmatrix} \tag{2}$$

$$\Delta[Hb_{total}] = \Delta[\mathrm{Hb}] + \Delta[\mathrm{HbO_2}] \tag{3}$$

where $\Delta \mathrm{OD}^{\lambda}$ is the change of optical density at wavelength λ, $\varepsilon_{\mathrm{Hb}}^{\lambda}$ and $\varepsilon_{\mathrm{HbO_2}}^{\lambda}$ are the extinction coefficients at wavelength λ for molar concentrations of [Hb] and [HbO_2], respectively, and L is the length of light path. Optical path length in a scattering medium L has been expressed as the source-detector separation d multiplied by a differential path length factor (DPF), *i.e.*, $L = d \times \mathrm{DPF}$ (14). Since we do not account for scattering effects, the units of $\Delta[Hb]$ and $\Delta[HbO_2]$ are mM/DPF (11).

NIRS was performed on a group of five pedicle tumor-bearing rats (~1 cm diameter). Rats were anesthetized with ketamine hydrochloride (120 μl; Aveco, Fort Dodge, IA) and maintained under general anesthesia (air and 1% isoflurane). The body temperature was maintained at ~37°C by a warm blanket. Prior to CA4P (n = 3) or saline (n = 2), NIRS was acquired for 10 min baseline measurement followed by 15 min oxygen breathing and 15 min upon return to air. Immediately after air reequilibration, CA4P (30 mg/kg) or saline (0.15 ml) was injected. Real time $\Delta[HbO_2]$ and $\Delta[Hb_{total}]$ were continuously monitored for 2 h, and then finally during another 15 min oxygen challenge. A follow-up study after 24 h was repeated with air and oxygen.

MRI experiments—A separate cohort of 9 tumor-bearing rats was used for MRI, which was performed using a 4.7 T Varian system. Each rat was given ketamine and maintained under general anesthesia (air and 1% isoflurane). A 27G butterfly was placed

intraperitoneally for infusion of CA4P or saline. A thermal blanket was used to maintain body temperature. Before, 2 h and 24 h after CA4P (30 mg/kg; n = 6) or saline (0.15 ml; n = 3) injection, diffusion-weighted (DW) spin echo multislice images were acquired over 8 mins on three 2 mm-thick tumor sections. Diffusion imaging parameters: TR = 2200 ms, TE = 90 ms, diffusion gradient pulses duration (Δ) = 25 ms, separation time of gradient pulse (δ) = 10 ms, b values = 22, 232 and 856 s/mm^2. Apparent diffusion coefficient (ADC) maps were generated using all three images by fitting DW images on a pixel-by-pixel basis to $S = S_0 \exp(-b*ADC)$, where S and S_0 are signal intensities with and without diffusive attenuation, respectively, and b is a factor that summarizes the gradient strength and timing used to generate the diffusion-weighted sequence. Data were processed on a voxel-voxel basis using IDL 5.3/5.4 (Research Systems, Boulder, CO).

For validation, a phantom study with a 1-cm-diameter plastic tube filled with water or saline was conducted at room temperature (21°C), and ADC values were obtained.

Experimental treatment

Radiation—*A* single dose of 5 Gy was given at a rate of 5 Gy/min using a clinical CyberKnife® system, composed of a compact 6 MV linear accelerator mounted on a robotic manipulator arm, coupled with 2 orthogonal x-ray imaging cameras (Accuray Inco, Sunnyvale, CA). Rats bearing pedicle tumors were placed on their side under general anesthesia (air or oxygen and 1% isoflurane). A piece of 2 × 2 × 1 cm SuperFlab bolus material (1.02g/cm^3 density, Radiation Products Design Inc., Albertville, MN) was placed directly over the tumor to improve dose uniformity. Use of stereotactic Cyberknife system ensured focusing radiation beam to cover tumor only.

Treatment groups—Animals bearing pedicle tumors were grouped as: 1) control (n = 5); 2) CA4P alone (30 mg/kg; n = 6); 3) radiation alone (IR; n = 6); 4) radiation while breathing oxygen (IR + O_2; n = 6); 5) radiation followed by CA4P 1 h later (IR + 1 h CA4P; n = 6); 6) radiation while breathing oxygen followed by CA4P 1 h later ((IR + O_2) + 1 h CA4P; n = 6); 7) CA4P followed by radiation 24 h later (CA4P + 24 h IR; n = 6); and 8) CA4P followed by radiation while breathing oxygen 24 h later (CA4P + 24 h (IR + O_2); n = 5). For oxygen intervention, the animals breathed oxygen (O_2 + 1% isofluorane) for 20 min before and during irradiation. Tumor sizes were measured every 3-7 days using a caliper and volume was calculated using the formula: volume = π/6 abc, where a, b and c are the three dimensions.

Histology and Immunohistochemistry

Tumor necrosis—Immediately following the 24 h MRI, three animals each from CA4P-treated tumors and saline controls were sacrificed. Tumor tissues were fixed in 10% formalin, embedded in paraffin and sectioned. Necrotic tumor regions were identified and analyzed on H&E stained slides of whole central tumor slices. The proportion of necrotic areas was calculated as the sum of all necrotic areas divided by total area using NIH ImageJ software.

Immunohistochemical detection of hypoxia—Hypoxia was assessed in nine tumor-bearing rats including six rats treated with CA4P and three with saline. After 24 h, the rats received *i.v.* infusion of hypoxia marker, pimonidazole (Hypoxyprobe™, HPI Inc.). Three of the CA4P rats breathed oxygen for 30 min before pimonidazole till sacrifice, while the other three breathed air throughout. Tumor specimens were immediately immersed in liquid nitrogen and stored at -80°C. Cryosections (10 μm thick) of the central tumor slice were immunostained for pimonidazole or vascular endothelium (CD31). An overnight incubation at 4°C with primary antibody Mab1 (1:100) or mouse anti-rat CD31 antibody (1:20; Serotec,

Raleigh, NC) was followed by 40 min with secondary FITC-conjugated goat anti mouse antibody (1:100; Jackson Lab, West Grove, PA) or Cy3-conjugated goat anti mouse antibody (1:100; Jackson Lab) at 37 °C. Pimonidazole positive staining was evaluated under 10× magnification, and the individual 10× fluorescence images were automatically stitched by using SoftWoRx (Applied Precision, Issaquah, WA). Hypoxic fraction was determined on the stitched whole pictures as area positively stained for pimonidazole relative to the total tissue area using the NIH ImageJ.

Statistical Analysis

Statistical significance was assessed using Student's *t*-tests. Analysis of variance (ANOVA) on the basis of Fisher's Protected Least Significant Difference (PLSD; Statview, SAS Institute, Inc., Cary, NC) was applied to compare mean changes at multiple time points following interventions, *i.e*, dynamic changes of NIRS or pixel-by-pixel ADC data.

Results

Monitoring CA4P effects *in vivo*

Near-infrared spectroscopy—NIRS revealed stable baseline $[HbO_2]$, $[Hb]$ and $[Hb_{total}]$ over 15 mins with air breathing (Fig. 1A and B). Immediately after switching to oxygen, a sharp increase followed by a further gradual increase in $\Delta[HbO_2]$ was evident and mirrored by a significant decrease in $\Delta[Hb]$ ($p < 0.0001$). Return to air breathing caused rapid return to status similar to baseline. After 15 minutes air re-equilibration, CA4P (30 mg/kg) or saline was injected. Both $\Delta[HbO_2]$ and $\Delta[Hb_{total}]$ dropped abruptly during the first ~ 20 min after CA4P and remained significantly low, indicating acute decrease in both vascular perfusion and oxygenation ($p < 0.0001$). Two hours after CA4P, switching to hyperoxic gas no longer elicited an increase in $\Delta[HbO_2]$. However, 24 h later, a significant increase in $\Delta[HbO_2]$ response to breathing oxygen was observed though the amplitude was lower than the baseline level ($p<0.001$; Fig. 1B). For the group of tumors treated with CA4P, mean normalized $\Delta[HbO_2]$ response to oxygen was 14 ± 11 (sd) % at 2 h, but recovered to 47 ± 22 (sd) % of the baseline level 24 h later ($p < 0.05$; Fig. 1C). For the saline control, NIRS showed stable values for all three parameters after saline infusion and typical response to oxygen in the whole course (Fig. 1A, C and D).

Diffusion-weight MRI—In phantom studies, Apparent diffusion coefficient (ADC) values of distilled water and saline were found to be 2.51×10^{-3} and 2.01×10^{-3} mm^2/s, respectively, at room temperature, which are in line with the observations reported by others. ADC maps of *in vivo* tumors revealed intratumoral heterogeneity, typically, with a central region showing higher ADC prior to treatment (Fig. 2A). CA4P caused a significant decrease in mean ADC of the representative tumor at 2 h (ADC = 0.83×10^{-3} mm^2/s), compared to the mean baseline = 0.93×10^{-3} mm^2/s ($p < 0.001$). Twenty-four hour follow-up showed enlargement of the areas of higher ADC at tumor center and a mean ADC = 1.02×10^{-3} mm^2/s, which was significantly higher than the baseline prior to CA4P ($p < 0.001$; Fig. 2). The 24 h ADC map correlated well with the histological section showing central necrosis and viable tumor tissue at periphery (Fig. 2A). Distribution of the ADC values showed a distinct left-shift at 2 h, while a right-shift was found 24 h later (Fig. 2B). For the group of tumors treated with CA4P ($n = 6$), significant decrease in mean ADC was observed at 2 h (1.03 ± 0.05 (se) $\times 10^{-3}$ mm^2/s; $p < 0.05$), which became significantly higher than the pretreatment level 24 h later ($1.26 \pm 0.05 \times 10^{-3}$ vs baseline = $1.16 \pm 0.07 \times 10^{-3}$ mm^2/s; $p < 0.05$; Fig. 3A). For the saline control group, there were no significant differences in ADC between each time point (Figs. 2B and 3A).

Histology and Immunohistochemistry

H&E staining showed significantly increased tumor necrosis 24 h post CA4P (42 ± 7%), as compared to saline treated tumors (20 ± 6%; $p < 0.05$; Figs. 2A and 3B). Pimonidazole staining in a saline control tumor showed sparse distribution of hypoxic regions (Fig. 4A). The central tumor sections of representative tumors obtained 24 h after CA4P showed numerous hypoxic regions (Fig. 4B), with much less hypoxia staining detected in a size-matched tumor that received oxygen inhalation (Fig. 4C). Quantitation of pimonidazole staining indicated significantly less hypoxia in oxygen-breathing tumors (22 ± 6%) than air-breathing tumors (49 ± 13%) 24 h post CA4P ($p < 0.05$; Fig. 4D).

Response to therapies

Tumor growth curves for the Control and 7 Treatment Groups are shown in Figure 5. A single dose of CA4P caused significant inhibition of tumor growth by day 3, compared to the control tumors, but they had caught up with the control tumors by day 7 ($p < 0.05$; Fig. 5 and Table 1). Irradiation alone (IR) caused a significant growth delay by day 3 and the tumors continued to grow more slowly than the control or CA4P-treated tumors. Among the various combination groups, the greatest tumor growth delay was achieved in the group treated with radiation plus oxygen breathing 24 h after CA4P (CA4P + 24 h (IR + O_2)). Table 1 summarizes relative tumor volume (RTV) in each group at different time points post treatment. After 14 days, when the rats in the other 6 Groups were sacrificed due to tumor ulceration, the CA4P + 24 h (IR + O_2) Group was alone significantly smaller than any other Group ($p < 0.05$; Table 1).

Discussion

In this study, we have applied non-invasive NIRS and DW MRI to evaluate tumor blood oxygenation and necrosis induced by CA4P. NIRS showed rapid decrease in vascular oxygenation and perfusion during the first 2 h post CA4P. Induction of central necrosis was evident by increased ADC 24 h later and confirmed by histology. The result of tumor hypoxiation induced by CA4P indicates that tumors, if treated with radiation shortly after VDA will probably be more radioresistant. Indeed, this has been confirmed in a number of preclinical studies comparing the sequence and interval between radiation and VDA (5). However, 24 h later increased $\Delta[HbO_2]$ (NIRS) and reduced pimonidazole staining with oxygen breathing indicated improved vascular perfusion and tumor oxygenation, consistent with our previous study using DCE MRI and ^{19}F NMR oximetry (7). Exploiting these observations, we now demonstrate that tumor oxygen dynamics and modulation of tumor hypoxia was manifested in the therapeutic response to the combination of CA4P and radiation.

DCE MRI has been widely applied to many tumor types with respect to VDAs previously, both in animal models and the clinic (15). NIRS utilizing endogenous hemoglobin provides a cheap, rapid and real-time monitoring of vascular oxygen dynamics in response to interventions. Recent clinical studies have demonstrated its usefulness in assessing breast cancer response to chemotherapy (16,17). Few previous studies have applied NIRS to detect tumor blood oxygenation following VDA, though Sunar *et al.* (18) showed that blood oxygen saturation decreased by 38% in mouse K1735 melanomas 1 h after CA4P treatment. However, Kragh *et al.* reported that CA4P caused no change in tumor blood volume of C3H mouse mammary tumors in foot pad even at a higher dose of 250 mg/kg (19), suggesting that differential responses to VDA may be tumor type dependent. Indeed, several reports indicate that tumor growing in mice require higher doses of CA4P to achieve vascular shutdown (20).

In contrast to the robust increase in $\Delta[HbO_2]$ with oxygen inhalation before CA4P, follow-up NIRS revealed little response at 2 h and small response 24 h after CA4P. This observation coincides with our previous DCE MRI studies of 13762NF tumors that showed CA4P-induced global reduction in vascular perfusion at 2 h (~80%), which recovered partially only in tumor periphery 24 h later, while the tumor center remained low (7). Our histological analysis of functional tumor vasculature by co-staining of vascular endothelium marker, CD31, and perfusion marker, Hoechst dye, confirmed the *in vivo* MRI observations (7). Thus, the observed hemoglobin dynamics in the current study reflected changes in vascular function induced by CA4P. Vascular shutdown at 2 h prevents oxygen delivery to the tumor, while smaller increase in $\Delta[HbO_2]$ at 24 h indicates partial recovery of vascular perfusion in the surviving rim.

Diffusion-weighted MRI, measuring the microscopic mobility of water can provide information about cellular structure, *i.e.*, cell density (12,13). ADC determined by DW MRI has been reported to correlate with cellular density, in which lower ADC values indicate higher cellularity, whereas necrotic tissue shows high ADC (13). Vascular perfusion also affects ADC. Significant decrease in ADC 2 h after CA4P reflected the decreased vascular perfusion, while increase in ADC 24 h later indicated the enlargement of the central necrotic core. These observations coincide with several other studies of VDA by DW MRI. Indeed, application of various ranges of b values, as reported in Thoeny's study (21), may facilitate differentiation of perfusion-sensitive ADC (low b values) from tissue-sensitive ADC (higher b values).

Hypoxia in solid tumors leads to resistance to radiotherapy and some anticancer drugs(6). ^{19}F MRI provides quantitative measurement and has great potential for preclinical studies (8,9). Our previous ^{19}F NMR oximetry studies have shown that the 13762NF tumors are relatively well oxygenated when small, typically having a hypoxic fraction (HF_{10}) less than 20% (7,22). Consistent with the low hypoxic fraction, a single dose of 5 Gy radiation caused a significant growth delay, but breathing oxygen produced no additional benefits when comparing IR alone with IR + O_2. Measurement of tumor pO_2 dynamics following CA4P was also conducted in our previous ^{19}F MRI study. Significant tumor hypoxiation was observed in 13762NF tumors with HF10 increasing from the baseline 30% to 80% 2 h post CA4P. However, oxygen breathing eliminated most hypoxic regions in the tumor periphery even though the pO_2 was significantly lower than pretreatment. Pimonidazole data in the current study also indicated significantly reduced hypoxia by inhaling oxygen 24 h after CA4P (Fig. 4). This was further demonstrated in the radiation results showing that the most significant tumor growth delay was found in the tumors treated with CA4P followed by radiation plus oxygen 24 h later.

We believe imaging can provide an important role in developing new drugs and evaluating novel therapeutic efficacy for pre-clinical investigation and ultimately to achieve personalized medicine. The present results further demonstrate that rational combination of CA4P + IR, while breathing oxygen generated enhanced tumor response. This suggests a role for oxygen sensitive measurements in developing combined therapy and potentially optimizing treatment of patients.

Acknowledgments

Supported by DOD Breast Cancer IDEA Awards 170310363 (DZ) and 170010459 (HL) and Pre-doctoral Award 170310353 (JG). Imaging infrastructure is provided by Southwestern Small Animal Imaging Research Program supported in part by U24 CA126608 and Simmons Cancer Center (P30 CA142543) and the Advanced Imaging Research Center (BTRP #P41-RR02584). CA4P was kindly provided by Dr. Dai Chaplin, Oxigene, Inc.

References

1. Denekamp J. Vascular attack as a therapeutic strategy for cancer. Cancer Metastasis Rev. 1990; 9:267–282. [PubMed: 2292139]
2. Horsman MR, Siemann DW. Pathophysiologic effects of vascular-targeting agents and the implications for combination with conventional therapies. Cancer Res. 2006; 66:11520–11539. [PubMed: 17178843]
3. Dark GG, Hill SA, Prise VE, et al. Combretastatin A-4, an agent that displays potent and selective toxicity toward tumor vasculature. Cancer Res. 1997; 57:1829–1834. [PubMed: 9157969]
4. Tozer, GM.; Kanthou, C.; Lewis, G., et al. Br J Radiol. Vol. 81. 2008. Tumour vascular disrupting agents: combating treatment resistance; p. S12-20.
5. Siemann DW, Rojiani AM. Enhancement of radiation therapy by the novel vascular targeting agent ZD6126. Int J Radiat Oncol Biol Phys. 2002; 53:164–171. [PubMed: 12007956]
6. Ansiaux R, Baudelet C, Jordan BF, et al. Mechanism of reoxygenation after antiangiogenic therapy using SU5416 and its importance for guiding combined antitumor therapy. Cancer Res. 2006; 66:9698–9704. [PubMed: 17018628]
7. Zhao D, Jiang L, Hahn EW, et al. Tumor physiologic response to combretastatin A4 phosphate assessed by MRI. Int J Radiat Oncol Biol Phys. 2005; 62:872–880. [PubMed: 15936572]
8. Zhao D, Jiang L, Mason RP. Measuring changes in tumor oxygenation. Methods Enzymol. 2004; 386:378–418. [PubMed: 15120262]
9. Jordan BF, Cron GO, Gallez B. Rapid monitoring of oxygenation by ^{19}F magnetic resonance imaging: Simultaneous comparison with fluorescence quenching. Magn Reson Med. 2009; 61:634–638. [PubMed: 19097235]
10. Kim JG, Zhao D, Song Y, et al. Interplay of tumor vascular oxygenation and tumor pO_2 observed using near-infrared spectroscopy, an oxygen needle electrode, and ^{19}F MR pO_2 mapping. J Biomed Opt. 2003; 8:53–62. [PubMed: 12542380]
11. Liu H, Gu Y, Kim JG, et al. Near-infrared spectroscopy and imaging of tumor vascular oxygenation. Methods Enzymol. 2004; 386:349–378. [PubMed: 15120261]
12. Padhani AR, Liu G, Koh DM, et al. Diffusion-weighted magnetic resonance imaging as a cancer biomarker: consensus and recommendations. Neoplasia. 2009; 11:102–125. [PubMed: 19186405]
13. Hamstra DA, Rehemtulla A, Ross BD. Diffusion magnetic resonance imaging: a biomarker for treatment response in oncology. J Clin Oncol. 2007; 25:4104–4109. [PubMed: 17827460]
14. Delpy DT, Cope M, van der Zee P, et al. Estimation of optical pathlength through tissue from direct time of flight measurement. Phys Med Biol. 1988; 33:1433–1442. [PubMed: 3237772]
15. Stevenson JP, Rosen M, Sun W, et al. Phase I trial of the antivascular agent combretastatin A4 phosphate on a 5-day schedule to patients with cancer: magnetic resonance imaging evidence for altered tumor blood flow. J Clin Oncol. 2003; 21:4428–4438. [PubMed: 14645433]
16. Zhu Q, Kurtzma SH, Hegde P, et al. Utilizing optical tomography with ultrasound localization to image heterogeneous hemoglobin distribution in large breast cancers. Neoplasia. 2005; 7:263–270. [PubMed: 15799826]
17. Jakubowski DB, Cerussi AE, Bevilacqua F, et al. Monitoring neoadjuvant chemotherapy in breast cancer using quantitative diffuse optical spectroscopy: a case study. J Biomed Opt. 2004; 9:230–238. [PubMed: 14715078]
18. Sunar U, Makonnen S, Zhou C, et al. Hemodynamic responses to antivascular therapy and ionizing radiation assessed by diffuse optical spectroscopies. Opt Express. 2007; 15:15507–15516. [PubMed: 19550836]
19. Kragh M, Quistorff B, Horsman MR, et al. Acute effects of vascular modifying agents in solid tumors assessed by noninvasive laser Doppler flowmetry and near infrared spectroscopy. Neoplasia. 2002; 4:263–267. [PubMed: 11988846]
20. Zhao D, Richer E, Antich PP, et al. Antivascular effects of combretastatin A4 phosphate in breast cancer xenograft assessed using dynamic bioluminescence imaging and confirmed by MRI. FASEB J. 2008; 22:2245–2451.

21. Thoeny HC, De Keyzer F, Chen F, et al. Diffusion-weighted MR imaging in monitoring the effect of a vascular targeting agent on rhabdomyosarcoma in rats. Radiology. 2005; 234:756–764. [PubMed: 15734932]

22. Song Y, Constantinescu A, Mason RP. Dynamic breast tumor oximetry: the development of prognostic radiology. Technol Cancer Res Treat. 2002; 1:471–478. [PubMed: 12625774]

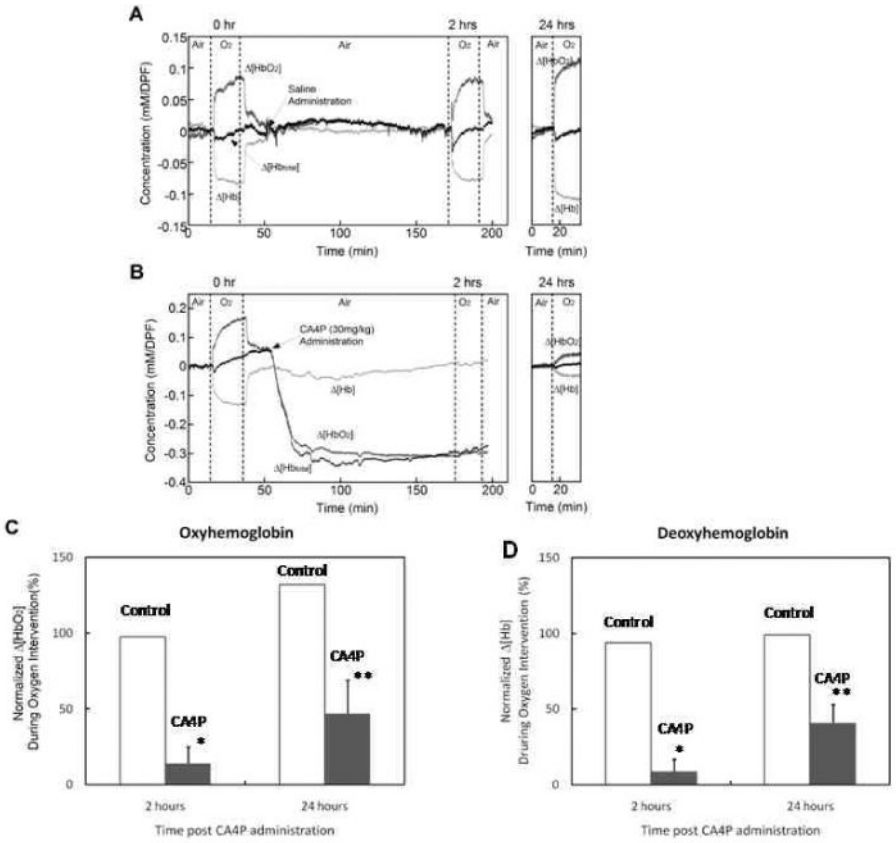

Figure 1. Near-infrared spectroscopy (NIRS) monitoring of tumor blood oxygenation in response to CA4P

A) For a control tumor, real-time NIRS revealed stable baseline and significant increase in oxyhemoglobin ($\Delta[HbO_2]$) observed immediately after switching from air to oxygen breathing ($p < 0.0001$). Mirrored by significantly decreased deoxyhemoglobin ($\Delta[Hb]$; $p < 0.0001$). Saline injection caused no marked change and reproducible oxygen response was observed 2 h and 24 h later. **B)** Following CA4P (30 mg/kg) administration, both $\Delta[HbO_2]$ and $\Delta[Hb_{total}]$ dropped rapidly with continuing decline for about 25 min, which remained at the lowest level 2 h post CA4P ($p < 0.001$). At this time, oxygen breathing no longer produced a significant increase in $\Delta[HbO_2]$. However, 24 h later, a small, but significant increase in $\Delta[HbO_2]$ was evident ($p < 0.005$). ANOVA Fisher's PLSD was used for testing statistic significance. **C)** Normalized oxyhemoglobin response to oxygen breathing at 2 h and 24 h was compared in the CA4P treated tumors ($n = 3$) and saline controls ($n = 2$). The amplitude change in $\Delta[HbO_2]$ was normalized to the baseline oxygen response, showing only 14 ± 11 (sd)% increase in $\Delta[HbO_2]$ at 2 h, but recovery to 47 ± 22 (sd)% of the baseline level 24 h later in CA4P treated tumors. **D)** Similarly, the normalized mean $\Delta[Hb]$ was plotted for CA4P or saline treated groups of tumors. * $p < 0.05$ to pretreatment, ** $p < 0.05$ to 2 h; paired Student's t-test.

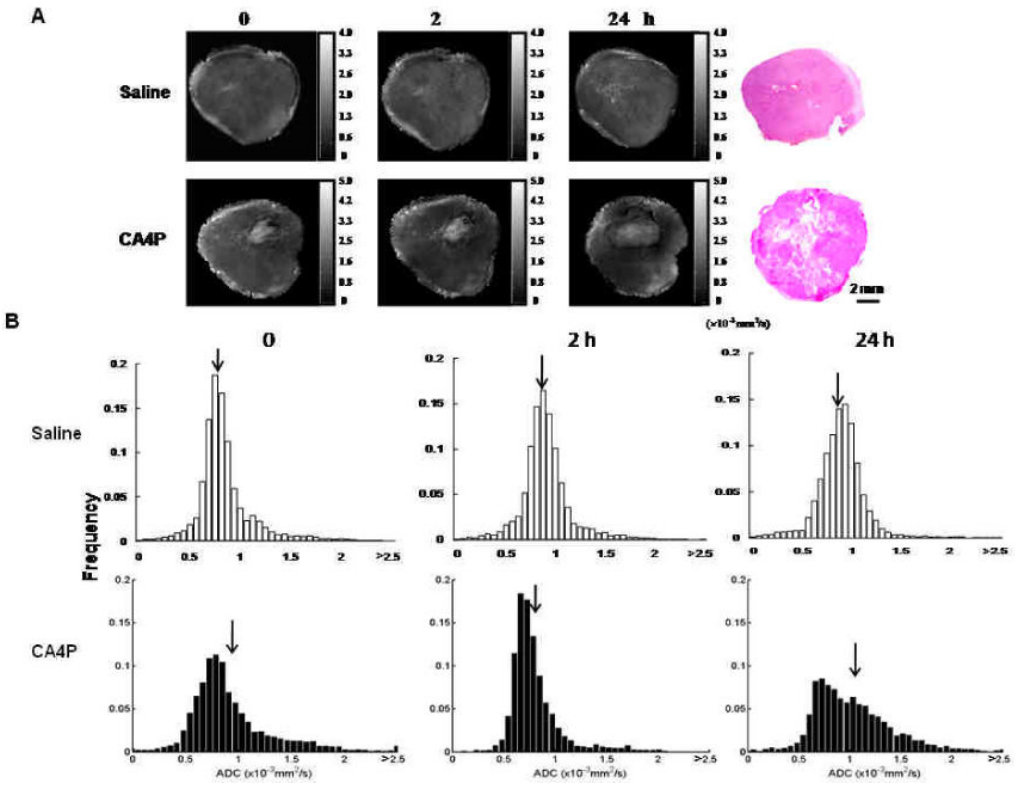

Figure 2. Diffusion weighted MRI evaluating tumor response to CA4P

A) ADC maps of representative tumors acquired at successive time points after saline or CA4P. In contrast to subtle differences observed in ADC maps of the saline control, the 2 h map of the CA4P-treated tumor contained more dark (low ADC) regions than pre-treatment, whereas there were many brighter regions (high ADC) at 24 h. Note: observation of bright pixels in tumor periphery may result from eddy currents, flow or motion artifacts. H&E staining of each tumor revealed larger central necrosis in the CA4P-treated tumor compared to the saline control tumor. **B)** Histograms of pixel-by-pixel ADC data (> 5000 pixels for each map) were plotted for the tumors presented in **A**. Relatively constant ADC distribution was observed for the saline control: baseline = 8.2, 2 h = 8.8 and 24 h = 8.7 × 10^{-3} mm^2/s, respectively. The CA4P-treated tumor showed a significant decrease in mean ADC at 2 h (mean = 0.83 × 10^{-3} mm^2/s). However, a significantly higher ADC was observed 24 h post treatment (mean = 1.02 × 10^{-3} mm^2/s), as compared to the baseline value (mean = 0.93 × 10^{-3} mm^2/s, $p < 0.001$; ANOVA Fisher's PLSD test). Arrows indicate mean values.

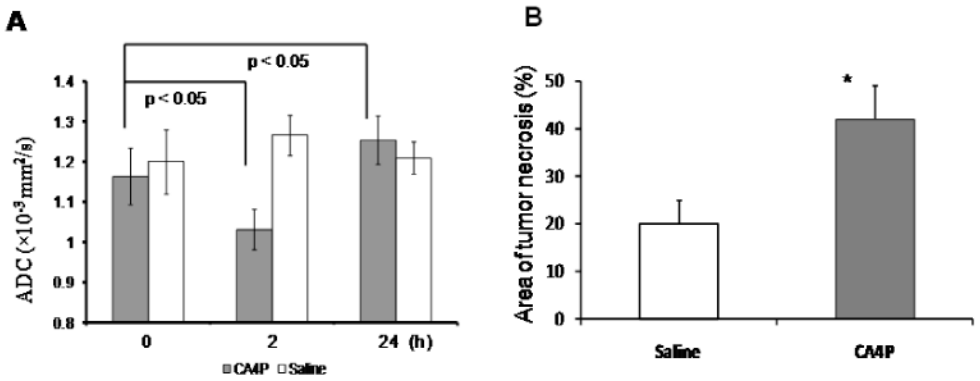

Figure 3. MRI of ADC and histological analysis of necrosis

A) Mean ± se ADC for the group of tumors treated with CA4P (n = 6) or saline control (n = 3) was plotted. Significant decrease in ADC at 2 h and then increase at 24 h after CA4P was evident ($p < 0.05$; paired Student's t-test). **B)** Quantitation of tumor necrosis on H&E sections showed significantly higher fractions of necrosis in CA4P-treated tumors than saline controls ($p < 0.05$; unpaired Student's t-test).

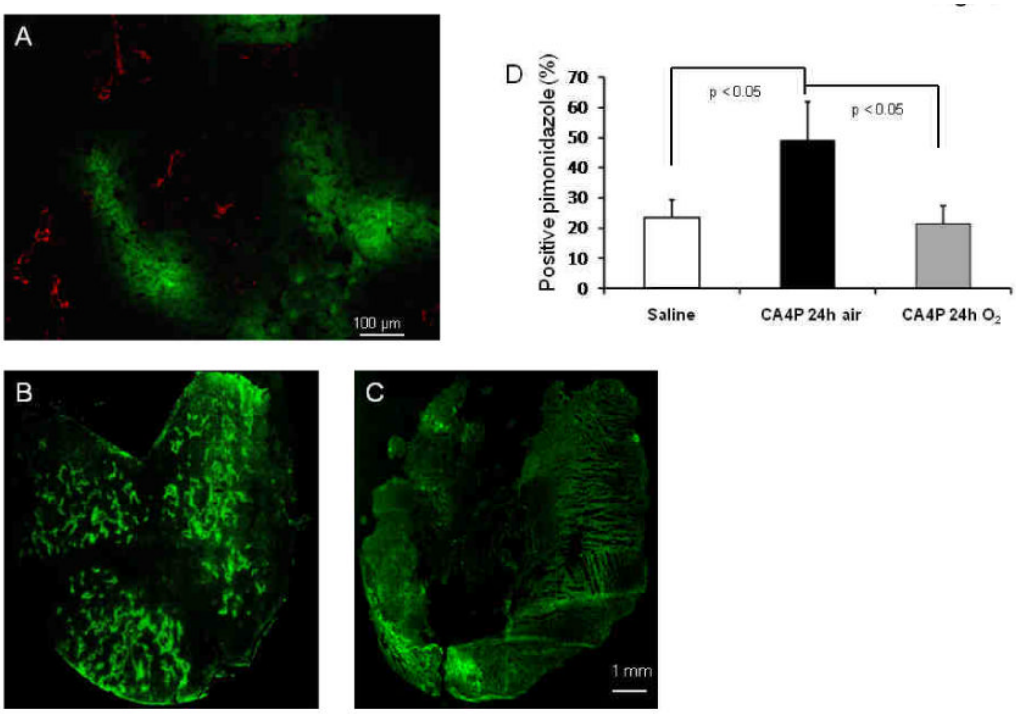

Figure 4. Pimonidazole staining of tumor hypoxia

A) Pimonidazole staining of a saline control tumor revealed hypoxic regions (green) are typically located distant from blood vessels (CD31, red). **B)** CA4P induced extensive tumor hypoxia 24 h later, as shown in a central tumor section. **C)** Much less tumor hypoxia was detected in an animal, which breathed oxygen 24 h after CA4P. **D)** Quantitation of pimonidazole staining indicated significantly increased hypoxia in CA4P-treat tumors (mean = 49 ± 13 (sd)% vs. 23 ± 6% (saline); $p < 0.05$; unpired Student's t-test), while markedly reduced hypoxia was observed in oxygen-treated tumors (22 ± 6 (sd)%; * $p < 0.05$).

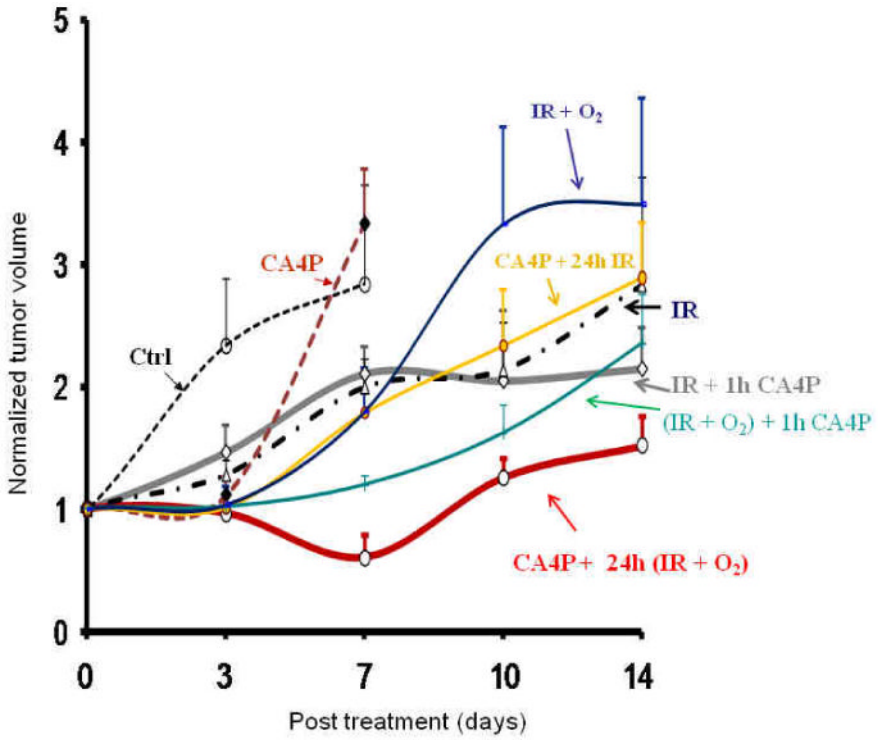

Figure 5. Tumor growth delay in response to various treatment regimens

Normalized mean tumor volume is shown for each treatment group. While a single dose of CA4P caused significant inhibition of tumor growth on day 3, the tumors rapidly caught up with the control tumors by day 7. Combined treatment provided little additional benefit on day3, but the tumors receiving combined therapy were all smaller than the Controls on day 7. The most significant tumor growth delay was seen in the tumors treated with CA4P followed by radiation plus oxygen 24 h later (CA4P + 24 h (IR + O_2)).

Table 1
Relative tumor growth with respect to treatment

	Relative tumor volume (RTV)		
Group	**Day 3**	**Day 7**	**Day 14**
Control	2.33 ± 0.55	2.84 ± 0.81	
CA4P	1.11 ± 0.14[a]	3.33 ± 0.45	
Radiation (IR)	1.28 ± 0.12[a]	2.00 ± 0.23	2.83 ± 0.88
IR + O_2	1.04 ± 0.14[a]	1.80 ± 0.35[a]	3.49 ± 0.87
CA4P + 24h IR	1.01 ± 0.11[a]	1.79 ± 0.29[a]	2.89 ± 0.45
IR + 1h CA4P	1.46 ± 0.22[a]	2.10 ± 0.23	2.14 ± 0.35
(IR + O_2) + 1h CA4P	1.02 ± 0.11[a]	1.20 ± 0.08[a,b]	2.35 ± 0.42
CA4P + 24h (IR + O_2)	0.96 ± 0.05[a,b]	0.60 ± 0.20[a,b]	1.51 ± 0.25[c]

[a] $p < 0.05$ from control;

[b] $p < 0.05$ from IR group;

[c] $p < 0.05$ from any of the other treatment groups (Student's t-test).

The animals in Control and CA4P alone were sacrificed on Day 7. CA4P was administered as a single dose of 30 mg/kg. IR was delievered as a single dose 5 Gy.